Surface excess properties from energy transport measurements during water evaporation

Fei Duan and C. A. Ward*

Thermodynamics and Kinetics Laboratory, Department of Mechanical and Industrial Engineering, University of Toronto, 5 King's College Road, Toronto, Ontario, Canada M5S 3G8

(Received 20 August 2004; revised manuscript received 21 March 2005; published 2 November 2005)

When water evaporates at high rates, recent studies indicate thermal conduction to the interface does not provide enough energy to evaporate water at the observed rate and that it is perhaps thermocapillary convection that transports the remaining energy. This possibility is examined by applying the Gibbs dividing-surface approximation to develop an expression for the energy transported along the interface. When this energy transport rate is compared with that required to evaporate the liquid at the observed rate, it is found that a Gibbs excess property, the "surface-thermal capacity," can be evaluated. A series of 19 evaporation experiments has been conducted under conditions for which there was no buoyancy-driven convection and for which the evaporation rate was progressively increased. For Marangoni numbers, (Ma) less than ~100, the interface was quiescent and thermal conduction (the Stefan condition) correctly predicted the energy transport rate to the surface. For experiments with $100 < \mathrm{Ma} < 22{,}000$, thermocapillary convection was present and the thermal conduction did not fully account for the energy transport. However, if the surface-thermal capacity is assigned a value of 30.6 ± 0.8 kJ/(m^2 K), then energy transport by thermocapillary convection and conduction provides the energy transport required to evaporate the liquid at the observed rate. For experiments with $\mathrm{Ma} > 22{,}000$, the interfacial flow was turbulent and viscous dissipation became important.

DOI: 10.1103/PhysRevE.72.056302 PACS number(s): 47.20.Dr

I. INTRODUCTION

A recent study [1] of the energy transport to the interface during steady-state water evaporation indicated that the energy transport by thermal conduction, under some conditions, accounts for as little as ~50% of the energy required to evaporate water at the measured rate. It was suggested that thermocapillary convection was responsible for the remainder of the energy transport. Although certain aspects of thermocapillary convection have been thoroughly studied [2–10], a quantitative method to predict the contribution of thermocapillary convection to the energy transport has not been established. The objective of this work is to use the Gibbs dividing-surface approximation [11] at a nonequilibrium interface and to evaluate experimentally the excess quantity that appears in the expression for the energy transport by thermocapillary convection and to determine if this excess quantity can be viewed as a property of a liquid-vapor interface.

The Gibbs description of a single-component, equilibrium system containing two fluid phases separated by a curved surface defines an excess number of moles, N^{LV}, and an excess internal energy U^{LV} and places the position of the dividing surface so the interface acts as a surface in tension [11]. For a nonequilibrium system, we define a local surface molar density n^{LV} (excess moles per unit surface area), surface internal energy u^{LV} (excess energy per excess mole), and specific heat of the excess energy, c^{LV}:

$$c^{LV} \equiv \left(\frac{\partial u^{LV}}{\partial T^{LV}} \right)_{n^{LV}}, \tag{1}$$

where T^{LV} is the temperature of surface phase [12]. The surface-thermal capacity is defined as $n^{LV}c^{LV}$ and is denoted by c_σ.

When the principles of energy and molar conservation are applied at a spherical liquid-vapor interface, where evaporation is taking place at a steady rate, we find a relation for the surface-thermal capacity and show that, provided thermocapillary convection is present and viscous dissipation is negligible, this excess quantity can be determined by measuring the rate of evaporation and the temperature profiles in the liquid and vapor phases. Its value is determined in each of nine experiments in which the evaporation flux is changed by a factor of ~34, and it is found to have the same value in each of the experiments. This suggests that the surface-thermal capacity is a surface property of the water-vapor interface that can be used when the Gibbs dividing-surface approximation is adopted to describe energy transport during phase change [13,14]. Physically, this property represents the capacity of the excess moles to store thermal energy.

II. EXPERIMENTAL APPARATUS AND PROCEDURE

The same experimental apparatus and procedures were used in this study as in [1]. Briefly, water was de-ionized, distilled, nanofiltered, and degassed (giving water with a resistivity of 18.2 MΩ-cm and a surface tension within 1% of the documented value). The prepared water was transferred directly into a syringe mounted in a syringe pump. The outlet of the syringe was connected by a stainless-steel tube to the throat of a stainless steel, conical funnel with a circular mouth that was enclosed in a vacuum chamber and con-

*Corresponding author. FAX: 416-978-7322. Electronic address: ward@mie.utoronto.ca

TABLE I. Thermal conditions measured in liquid and vapor-phases during steady-state evaporation.

Experiment	EV1	EV2	EV3	EV4	EV5	EV6	EV7	EV8	EV9	EV10
Vap.-Ph. Press. (Pa)	797.2 ±13.3	795.7 ±13.3	786.8 ±13.3	791.9 ±13.3	787.9 ±13.3	786.6 ±13.3	783.9 ±13.3	777.3 ±13.3	770.1 ±13.3	765.3 ±13.3
Intf. Ht.[a] (mm)	0.98 ±0.01	1.00 ±0.01	0.98 ±0.01	0.99 ±0.01	1.01 ±0.01	1.03 ±0.01	0.97 ±0.01	1.00 ±0.01	0.97 ±0.01	1.00 ±0.01
Avg. Evap. Flux (g/m^2s)	0.027 ±0.001	0.034 ±0.001	0.044 ±0.001	0.050 ±0.001	0.057 ±0.001	0.063 ±0.001	0.070 ±0.001	0.100 ±0.001	0.134 ±0.002	0.200 ±0.002
Throat temp. (°C)	3.52 ±0.03	3.60 ±0.03	3.54 ±0.03	3.56 ±0.03	3.56 ±0.03	3.57 ±0.03	3.53 ±0.03	3.53 ±0.03	3.48 ±0.03	3.57 ±0.04
T_I^V (°C)[a]	4.95 ±0.02	4.88 ±0.02	4.62 ±0.02	4.65 ±0.02	4.68 ±0.02	4.62 ±0.02	4.56 ±0.02	4.46 ±0.02	4.35 ±0.02	4.20 ±0.02
T_I^L (°C)[a]	3.70 ±0.02	3.76 ±0.02	3.52 ±0.02	3.57 ±0.02	3.56 ±0.02	3.56 ±0.02	3.47 ±0.02	3.35 ±0.02	3.26 ±0.02	3.11 ±0.02
Unif.-temp. layer[a] (mm)								0.80 ±0.02	0.63 ±0.02	0.43 ±0.02
Max. tangential speed (mm/s)	0.00 ±0.00	0.00 ±0.00	0.00 ±0.00	0.00 ±0.00	0.00 ±0.00	0.00 ±0.00		0.22 ±0.00	0.26 ±0.00	0.31 ±0.01
Marangoni No., Ma	−474	−443	38	3	5	10	127	447	641	1,198

[a]On the center line.

nected to two pumping systems: a turbomolecular pump and its backing pump and a separate mechanical pump. The chamber could be monitored with a mass spectrometer.

Before an experiment, the chamber and syringe were evacuated for 12 h to a pressure of about 10^{-5} Pa. The prepared water was then admitted to the syringe and pumped up to the funnel mouth. The funnel mouth was visible from outside the chamber, and the height of the water-vapor interface could be monitored with two cathetometers that had a viewing angle between them of 90°. To prevent subsequent bubble formation, with water filling the funnel, the chamber was pressurized with N_2 to 42.0 kPa for 6 h. Afterwards, ~2 ml of the water in the syringe was flushed out and into the chamber. The chamber was then evacuated with the mechanical vacuum pump until dry. Water was pumped into the funnel until the maximum height of the water-vapor interface above the funnel mouth was approximately 1 mm. A cooling system allowed the water at the funnel *throat* to be maintained at ~3.6 °C (see Table I).

The temperature in the vapor and liquid phases could be measured with a calibrated thermocouple (type K) that had been formed into a U shape. The bottom of the U shape was 1 mm in length with the junction in the middle. The thermocouple wire was 25.4 μm in diameter and mounted on a three-dimensional positioner. Two cathetometers, separated by an angle of 90°, were used with the positioner to determine the horizontal and vertical locations of the thermocouple bead with an accuracy of ±10 μm. The temperature was measured in one horizontal direction at 0.0, 0.7, 1.4, 2.1, 2.8, and 3.15 mm from the center line of the funnel, and at each horizontal position, the thermocouple was placed at several vertical positions. Near the interface, the distance between two measurements in the vertical direction was 10 μm in the vapor phase and 20 μm in the liquid phase. At each position, the thermocouple reading was recorded each second for a period of 1 min (by a Labview program using a 34970A HP data acquisition/switch unit) and the mean and standard deviations of the temperature at each position calculated. The pressure in the vapor phase was measured approximately 20 cm above the funnel mouth with a Hg manometer.

III. EXPERIMENTAL RESULTS

A summary of the conditions under which the experiments were conducted is presented in Table I, and for comparison, the conditions under which the experiments reported in [1] were performed are listed in Table II. The basic difference between these two sets of experiments is only the evaporation rate, but this gave rise to significant changes in the mechanism of energy transport.

The experiments can be parametrized in terms of the Marangoni and Rayleigh numbers. If the surface tension is denoted by γ^{LV}, the temperature of the water at the funnel throat by T_t^L, the temperature on the center line at the liquid-vapor interface by T_{0I}^L, the thermal diffusivity of the liquid by α_L, the dynamic viscosity by η, and the distance on the center line from the throat thermocouple to the liquid-vapor interface by D, the Marangoni number can be expressed

$$\mathrm{Ma} = \left(\frac{\partial \gamma^{LV}}{\partial T}\right)_I \frac{(T_{0I}^L - T_t^L)D}{\alpha_L \eta}. \tag{2}$$

If the expansivity of water is denoted as β, the gravitational acceleration by g, and the density by n^L, then the Rayleigh number may be written

TABLE II. Thermal conditions measured in liquid and vapor-phases during steady-state evaporation [1].

Experiment	EV11	EV12	EV13	EV14	EV15	EV16	EV17	EV18	EV19
Vap.-Ph.	745.3	665.3	591.9	505.3	398.6	301.3	285.3	264.0	258.6
Press. (Pa)	±13.3	±13.3	±13.3	±13.3	±13.3	±13.3	±13.3	±13.3	±13.3
Intf. Ht.[a]	1.00	1.05	1.01	0.96	1.00	1.01	1.00	0.99	1.00
(mm)	±0.01	±0.01	±0.01	±0.01	±0.01	±0.01	±0.01	±0.01	±0.01
Avg. Evap.	0.407	1.002	1.371	1.788	2.544	3.378	3.026	3.421	4.242
Flux (g/m^2s)	±0.006	±0.011	±0.015	±0.018	±0.025	±0.031	±0.028	±0.032	±0.039
Throat	3.52	3.51	3.59	3.56	3.60	3.54	3.59	3.57	3.59
temp (°C)	±0.05	±0.05	±0.04	±0.03	±0.04	±0.03	±0.05	±0.03	±0.10
T_I^V (°C)[a]	4.73	3.37	1.84	−0.20	−2.65	−5.66	−7.19	−7.31	−7.59
	±0.02	±0.02	±0.05	±0.05	±0.05	±0.02	±0.04	±0.08	±0.06
T_I^L (°C)[a]	2.73	1.11	−0.53	−2.82	−6.04	−9.67	−11.61	−11.86	−12.06
	±0.03	±0.02	±0.03	±0.03	±0.03	±0.03	±0.03	±0.03	±0.04
Unif.-temp.	0.35	0.17	0.13	0.09	0.07	0.07	0.05	0.05	0.05
layer[a] (mm)	±0.01	±0.01	±0.01	±0.01	±0.01	±0.01	±0.01	±0.01	±0.01
Max. tangential	0.24	0.44	0.51	0.50	0.59	0.65	1.15	0.94	0.91
speed (mm/s)	±0.01	±0.01	±0.02	±0.01	±0.01	±0.01	±0.04	±0.02	±0.03
Marangoni No., Ma	2,155	6,018	9,601	13,533	18,208	21,472	22,410	22,462	22,596

[a]On the center line.

$$\mathrm{Ra} = \frac{g n^L \beta (T_{0I}^L - T_t^L) D^3}{\alpha_L \eta}. \tag{3}$$

The calculated value of Ma for each experiment is listed in Tables I and II.

The type of results obtained when Ma $<$ 100 (Table I) is illustrated in Fig. 1 where the measurements of experiment EV5 are shown. Since the conditions under which the evaporation took place from the circular funnel mouth were approximately axisymmetric, we have only presented the measurements made at six horizontal positions in one direction. Note that as a function of *depth*, the temperature in the liquid was uniform at each horizontal position, but there was a temperature gradient in the vapor phase, indicating that the liquid was being heated from above (by the surroundings). These characteristics were shared by six experiments (EV1–EV6, Table I). For example, the temperature measured tangential to the interface in EV5 is shown in Fig. 2. There was no measurable gradient in the interfacial liquid temperature

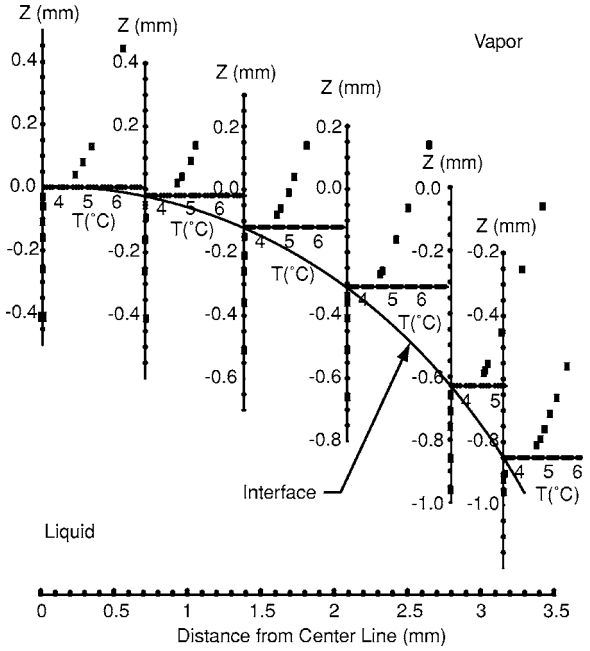

FIG. 1. Temperature measured across the phase boundary at six horizontal positions as water evaporates under steady-state conditions at an average flux of 0.057 $g/(s\,m^2)$, Table I, EV5.

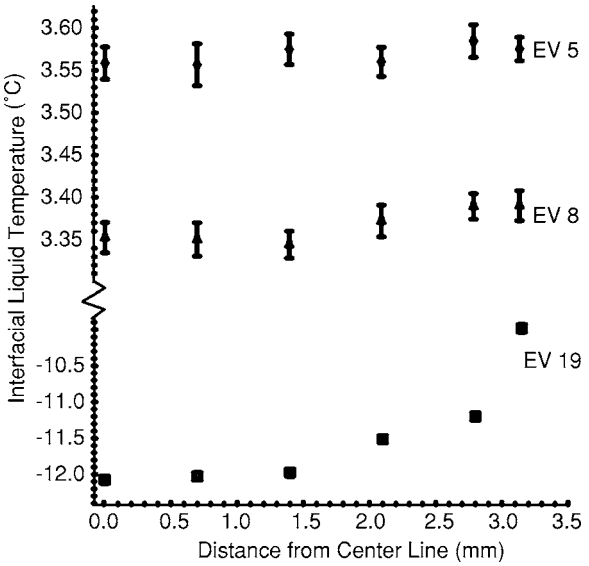

FIG. 2. The interfacial liquid temperature measured as a function of distance from the center line of the funnel in three different experiments. The conditions in each experiment are listed in Tables I and II. For EV5, Ma $<$ 100; for EV8, Ma $>$ 100; and for EV19, Ma $>$ 22,000. The evaporation flux of each experiment is indicated.

and no uniform-temperature layer immediately below the interface [1,15], and the gradient in the liquid temperature with depth was small. Note that for EV1 and EV2, the temperature at the funnel throat was slightly *less* than that on the center line at the liquid-vapor interface, giving a negative value for Ma. In both of these experiments, there was evaporation, but the heating by the surroundings at the interface overcame the effect of evaporative cooling. The value of the Rayleigh number for EV1 and EV2 was 2.3 and 1.7, respectively, values that are far below the critical value for buoyancy-driven convection ($\sim$1,100).

The evaporation rate was progressively increased for experiments EV7–EV16, and Ma increased so that it was in the range $100 < \mathrm{Ma} < 22{,}000$, but there was no buoyancy-driven convection in any experiment. The temperature at the interface was less than that at the funnel throat, and the latter was less than 4 °C. Since water has it maximum density at 4 °C and its density decreases monotonically as the temperature decreases below 4 °C, the lighter liquid was at the top of the funnel ($\mathrm{Ra} < 0$) and there could not have been any buoyancy-driven convection. Similarly, in the vapor, the coldest vapor was in contact with the liquid and therefore at the bottom of the vapor phase. Thus there could not have been any buoyancy-driven convection in this phase either. A temperature discontinuity was found to be present at the interface in which the interfacial vapor temperature was greater than that of the liquid phase. Similar discontinuities have been previously reported [13–20].

As indicated in Table I, when Ma was 447 or higher, a uniform-temperature layer of measurable thickness was present immediately below the interface. The thickness of this layer decreased as the evaporation rate was increased [15]. This relation between the evaporation rate and the thickness of the uniform-temperature layer has been observed previously [1,15]. As may be seen in Fig. 2, a steady-state gradient in the interfacial liquid temperature did exist for the experiments with Marangoni numbers in this range. The temperature at the funnel throat was controlled at a temperature near but below 4 °C; thus, thermal energy would have been conducted through the stainless steel funnel to the funnel rim where it would have gone into heating the liquid. As will be seen, this energy was distributed along the interface by thermocapillary convection.

For experiments EV17–EV19, Ma was greater than 22,000 and there was also a strong gradient in the interfacial liquid temperature. Evidence is discussed in [1] that indicates the interfacial flow for these experiments was turbulent (see below).

IV. DATA ANALYSIS

In the experiments described in Tables I and II, the liquid-vapor interface had a maximum height above the funnel mouth of $\sim$1 mm and the measured height of the interface was within 1% of the calculated spherical height; thus, to describe the interface, we will use spherical coordinates (r, θ, ϕ, where ϕ is the azimuthal angle about the axis $\theta=0$).

We adopt the Gibbs dividing-surface approximation to describe the interfacial region, take the position of the dividing surface to have a radius R_0, and consider an element of the surface. The excess internal energy U^{LV} of the surface element is assumed to have as its independent variables the excess entropy S^{LV}, the surface area A^{LV}, and the excess number of moles, N^{LV}, of the element and is required to be a first-order homogeneous function. Then,

$$dU^{LV} = T^{LV} dS^{LV} + \gamma^{LV} dA^{LV} + \mu^{LV} dN^{LV}, \tag{4}$$

where the definitions of the temperature and surface tension are given by

$$\gamma^{LV} \equiv \left(\frac{\partial U^{LV}}{\partial A^{LV}} \right)_{S^{LV}, N^{LV}}, \quad T^{LV} \equiv \left(\frac{\partial U^{LV}}{\partial S^{LV}} \right)_{A^{LV}, N^{LV}},$$

$$\mu^{LV} \equiv \left(\frac{\partial U^{LV}}{N^{LV}} \right)_{S^{LV}, A^{LV}}.$$

The first-order homogeneous-function property of U^{LV} and the definition of the intensive properties lead to an Euler-type relation for the surface phase,

$$U^{LV} - T^{LV} S^{LV} - \gamma^{LV} A^{LV} = \mu^{LV} N^{LV}, \tag{5}$$

and allows the intensive surface energy u^{LV}, the internal energy per excess mole, to be written in terms of the intensive surface entropy σ^{LV} (entropy per excess mole) and intensive surface area α^{LV} (surface area per excess mole—i.e., $1/n^{LV}$):

$$u^{LV} = u^{LV}(\sigma^{LV}, \alpha^{LV}). \tag{6}$$

Then one can show that

$$du^{LV} = T^{LV} d\sigma^{LV} + \gamma^{LV} d\alpha^{LV}, \tag{7}$$

and that

$$d\mu^{LV} = -\sigma^{LV} dT^{LV} - \alpha^{LV} d\gamma^{LV}. \tag{8}$$

Equations (7) and (8) are applied below.

Since under steady-state conditions there are no net changes in the number of moles in a surface element, the moles transported into the surface element must be equal to those transported out. If the velocity in bulk phase k (L or V) evaluated at the surface is denoted as $\boldsymbol{\nu}_I^k$ and those of the excess number of moles by $\nu_\theta^{LV} \boldsymbol{i}_\theta$ and $\nu_\phi^{LV} \boldsymbol{i}_\phi$, then

$$n^L \boldsymbol{\nu}_I^L \cdot \boldsymbol{i}_r = n^V \boldsymbol{\nu}_I^V \cdot \boldsymbol{i}_r + \boldsymbol{\nabla}(n^{LV} \nu_\theta^{LV}) \cdot \boldsymbol{i}_\theta + \boldsymbol{\nabla}(n^{LV} \nu_\phi^{LV}) \cdot \boldsymbol{i}_\phi, \tag{9}$$

where the subscript I on a quantity indicates it is to be evaluated at the interface. We shall assume the local evaporation flux j_{ev} may be expressed as

$$j_{ev} = n_I^L \boldsymbol{\nu}_I^L \cdot \boldsymbol{i}_r = n_I^V \boldsymbol{\nu}_I^V \cdot \boldsymbol{i}_r. \tag{10}$$

This ensures that there is not any change in the molar storage in the surface phase as the evaporation continues. Then Eq. (9) reduces to

$$\boldsymbol{\nabla}(n^{LV} \nu_\theta^{LV}) \cdot \boldsymbol{i}_\theta + \boldsymbol{\nabla}(n^{LV} \nu_\phi^{LV}) \cdot \boldsymbol{i}_\phi = 0. \tag{11}$$

The conservation of energy principle applied in the steady-state circumstance requires that the energy transport into the surface element must equal the sum of that leaving and that being dissipated by viscosity in the surface, Φ_I ($\mathrm{J/m^2}$):

$$(n^L h^L \boldsymbol{\nu}^L - \kappa^L \nabla T^L)_I \cdot \boldsymbol{i}_r = (n^V h^V \boldsymbol{\nu}^V - \kappa^V \nabla T^V)_I \cdot \boldsymbol{i}_r + \Phi_I + [n^{LV} \nu_\theta^{LV} (\nabla u^{LV})_I + u^{LV} \nabla (n^{LV} \nu_\theta^{LV})_I] \cdot \boldsymbol{i}_\theta + [n^{LV} \nu_\phi^{LV} (\nabla u^{LV})_I + u^{LV} (\nabla (n^{LV} \nu_\phi^{LV}))_I] \cdot \boldsymbol{i}_\phi. \quad (12)$$

After making use of Eqs. (10) and (11), one finds

$$j_{ev}(h^V - h^L)_I = (\kappa^V \nabla T^V - \kappa^L \nabla T^L)_I \cdot \boldsymbol{i}_r - \frac{n^{LV} \nu_\theta^{LV}}{R_0} \left(\frac{\partial u^{LV}}{\partial \theta} \right)_\phi - \frac{n^{LV} \nu_\phi^{LV}}{R_0 \sin\theta} \left(\frac{\partial u^{LV}}{\partial \phi} \right)_\theta - \Phi_I. \quad (13)$$

We note that the term on the left of Eq. (13) is the local energy transport required to evaporate the liquid, the first term on the right is the energy transported locally to the interface by thermal conduction, and the second and third terms are the local transport of energy by thermocapillary convection and the local energy dissipation.

A. Evaporation when Ma < 100

If there were no thermocapillary convection, ν_θ^{LV}, ν_ϕ^{LV}, and Φ_I would vanish and the energy to evaporate the liquid could be supplied only by thermal conduction. Equation (13) then reduces to the conventional Stefan condition

$$j_{ev}(h^V - h^L)_I = (\kappa^V \nabla T^V - \kappa^L \nabla T^L)_I \cdot \boldsymbol{i}_r. \quad (14)$$

To determine the conditions under which thermocapillary convection may be neglected, we compare the rate of energy transport required to evaporate the liquid at the measured rate, $\dot{E}_{ev}$, with the net rate of the thermal conduction to the surface, $\dot{Q}_N$. The former is given by

$$\dot{E}_{ev} = 2\pi \int_0^{\theta_m} j_{ev}(h^V(T_I^V) - h^L(T_I^L)) R_0^2 \sin\theta \, d\theta, \quad (15)$$

where θ_m is the maximum value of the polar angle. Since the radius of the cone mouth is 3.5 mm,

$$\theta_m = \arcsin(3.5 \text{ mm}/R_0),$$

and the thermal conduction to the surface, $\dot{Q}_N$, may be expressed as

$$\dot{Q}_N = 2\pi \int_0^{\theta_m} [(\kappa^V \nabla T^V - \kappa^L \nabla T^L)_I \cdot \boldsymbol{i}_r] R_0^2 \sin\theta \, d\theta. \quad (16)$$

The variation in $(h^V(T_I^V) - h^L(T_I^L))$ along the interface in any particular experiment was less than 1.0%, but this quantity varies from one experiment to another because of the change in temperature at the interface. Thus Eq. (15) gives, for a particular experiment,

$$\dot{E}_{ev} = J_{ev}(h^V(T_I^V) - h^L(T_I^L)). \quad (17)$$

where J_{ev} is the measured rate of evaporation. The temperature was measured in the vertical direction at different positions along the interface (Fig. 1). From it, the thermal flux normal to the interface may be written in terms of spherical coordinates at these points:

$$\left[\kappa^V \left(\frac{\partial T^V}{\partial r} \right)_I - \kappa^L \left(\frac{\partial T^L}{\partial r} \right)_I \right] = \frac{1}{\cos\theta} \left[\kappa^V \left(\frac{\partial T^V}{\partial z} \right)_I - \kappa^L \left(\frac{\partial T^L}{\partial z} \right)_I \right]. \quad (18)$$

The measured value of the conductive flux normal to the interface at each interfacial position obtained from Eq. (18) for each experiment was assumed to be expressible in terms of a polynomial in $\cos\theta$:

$$\left[\kappa^V \left(\frac{\partial T^V}{\partial r} \right)_I - \kappa^L \left(\frac{\partial T^L}{\partial r} \right)_I \right] = c_0 + c_1 \cos\theta + c_2 \cos^2\theta + c_3 \cos^3\theta. \quad (19)$$

The values of c_j $(0 \leqslant j \leqslant 3)$ were determined from the measured temperature gradient for each experiment. The measured thermal fluxes normal to the interface in each of the 19 experiments may be compared with that calculated from Eq. (19) in Fig. 3. The thermocouple could not be placed at the full diameter of the funnel mouth. The extrapolated portion of the calculated thermal flux normal to the interface is shown as a dashed line for each experiment in this figure.

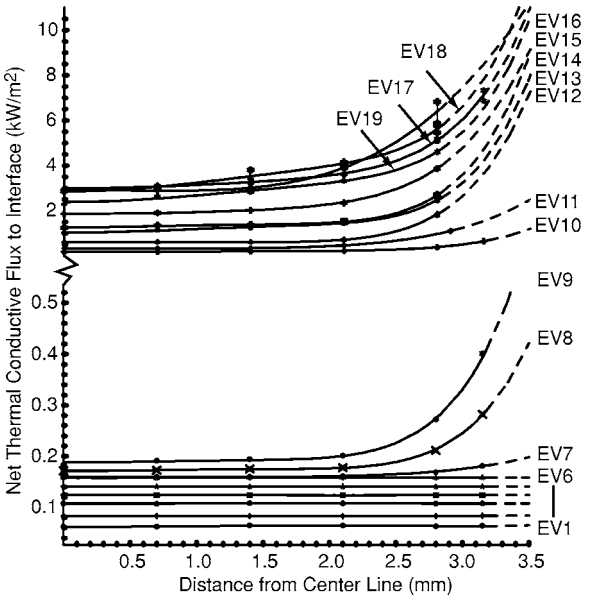

FIG. 3. Calculated net thermal conduction flux to the interface for experiments EV1–EV19. The experimental conditions are listed in Table I.

Once the values of c_j have been established, the value of the net, total conductive flux normal to the interface, $\dot{Q}_N$, is given by

$$\dot{Q}_N = 2\pi R_0^2 \int_0^{\theta_m} (c_0 + c_1 \cos\theta + c_2 \cos^2\theta + c_3 \cos^3\theta) \sin\theta \, d\theta. \quad (20)$$

In Fig. 4, the calculated values of $\dot{Q}_N$ are compared with $\dot{E}_{ev}$ for 16 of the experiments described in Tables I and II. As

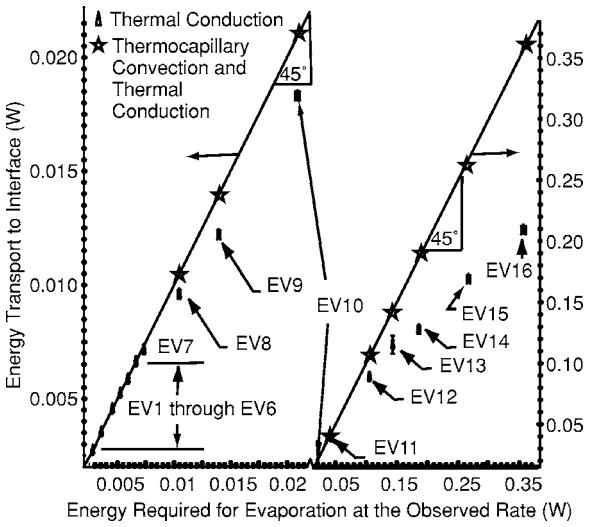

FIG. 4. Comparison of the rate of energy transport to the interface by thermal conduction with that required to evaporate the liquid at the measured rate. There is complete agreement between the two rates for experiments EV1–EV6, but for EV7 and those with a higher evaporation rate, thermal conduction does not provide enough energy to evaporate the liquid at the measured rate. When energy transport by both thermal conduction and by thermocapillary convection are taken into account, the energy conservation principle is completely satisfied.

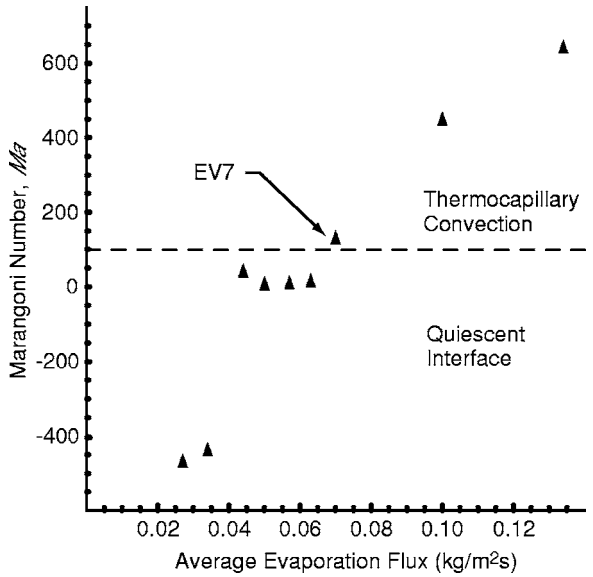

FIG. 5. The results in Fig. 4 and in this figure indicate the critical Marangoni number $\mathrm{Ma}_{\mathrm{Cr}}$ for the transition from a quiescent interface to one with thermocapillary convection is in the range $38 < \mathrm{Ma}_{\mathrm{Cr}} < 127$. Experiment EV7 is the experiment with the lowest Ma for which the thermal conduction does not provide enough energy to evaporate the liquid at the observed rate.

may be seen there, for EV1–EV6 almost complete agreement exists between $\dot{Q}_N$ and $\dot{E}_{ev}$. For these six experiments, Ma < 100 and the results suggest that the thermocapillary convection was negligible or nonexistent. Thus, when there is no thermocapillary convection, these results indicate that the conventional Stefan condition gives a valid description of the energy transport required to evaporate the liquid.

B. Evaporation when $100 < \mathrm{Ma} < 22{,}000$

For experiments EV8–EV16, as indicated in Fig. 4, the energy transported to the interface by thermal conduction is less than that required to evaporate the liquid at the observed rate, and as the evaporation rate is progressively increased, the deficit progressively increases. The results in Figs. 4 and 5 suggest that the critical Ma for the transition from a quiescent interface to one where thermocapillary convection is present is in the range $38 < \mathrm{Ma}_{\mathrm{Cr}} < 127$.

When $\mathrm{Ma} \geqslant 127$, the results in Fig. 4 indicate that thermocapillary convection cannot be neglected. Nonetheless, the measured temperature profile showed no dependence on ϕ, indicating that the thermocapillary convection in the $\boldsymbol{i}_\phi$ direction was negligible. The expression for ν_θ^{LV} was determined in [1] by equating the gradient in the surface tension in the $\boldsymbol{i}_\theta$ direction, $\nabla\gamma^{LV}\cdot\boldsymbol{i}_\theta$, to the viscous stress in that direction, $\sigma_{r\theta}(R_0,\theta)$. This gave a differential equation that could be approximately integrated to give

$$\nu_\theta^{LV}(R_0,\theta) = -\frac{1}{\eta}\left(\frac{d\gamma^{LV}}{dT^L}\right)_I \left(\frac{\partial T_I^L}{\partial\theta}\right)_\phi \ln\left(1-\frac{\delta_u}{R_0}\right), \qquad (21)$$

where δ_u is the thickness of the uniform-temperature layer and η is the viscosity of the liquid phase. The validity of this expression for the thermocapillary flow was examined by comparing the value predicted from Eq. (21) with the value inferred from flow probe measurements [1]. The probe was a 12.7-μm-diam cylinder. One end was mounted as a cantilever, and the other end was inserted 40 μm into the liquid as it evaporated under steady-state conditions. From the measured deflection, the drag force resulting from the thermocapillary flow could be determined, and using an analytical expression for the drag, the thermocapillary flow speed was determined. The comparison indicated that the flow speed calculated from Eq. (21) agreed reasonably with that obtained from the probe-deflection measurements. But we emphasize that the speed calculated from Eq. (21) is the mean fluid speed. The probe measurements clearly indicated that there were fluctuations in the flow speed: immediately upon touching the evaporating liquid, the probe deflected, but then it oscillated about the deflected position. These flow fluctuations are important in determining the properties of the surface phase (see below).

For the experiments in the range of Marangoni numbers being considered, a uniform-temperature layer existed below the interface (Tables I and II) and had an extent of $0.07 \leqslant \delta_u \leqslant 0.80$ mm depending on the distance from the center line and the evaporation rate. Following [1] we take the expression for δ_u to be

$$\delta_u = b_0 + b_1 \sin^2\theta + b_2 \sin^4\theta \qquad (22)$$

and determine the values of b_i $(0 \leqslant i \leqslant 2)$ numerically. We take the temperature measured in the uniform-temperature layer to be the temperature of the surface phase, T^{LV}, and of the liquid at the interface, T_I^L [12]:

$$T_I^L = a_0 + a_1 \sin^2 \theta. \tag{23}$$

The measured values of this temperature at each interfacial position of each experiment were used to determine the values of a_0 and a_1.

An estimate of the magnitude of the terms in Eq. (13) indicates that the viscous dissipation Φ_I can be neglected. We proceed by neglecting this term and consider this assumption again in view of the results obtained. Hence Eq. (13) reduces to

$$(\kappa^V \nabla T^V - \kappa^L \nabla T^L)_I \cdot \mathbf{i}_r = j_{ev}(h^V - h^L) + \frac{n^{LV}\nu_\theta^{LV}}{R_0}\left(\frac{\partial u^{LV}}{\partial \theta}\right)_\phi. \tag{24}$$

From Eq. (7), one finds

$$\left(\frac{\partial u^{LV}}{\partial \theta}\right)_\phi = c^{LV}\left(\frac{\partial T_I^L}{\partial \theta}\right)_\phi + \left[\gamma^{LV} + T_I^L\left(\frac{\partial \sigma^{LV}}{\partial \alpha^{LV}}\right)\right]\left(\frac{\partial \alpha^{LV}}{\partial \theta}\right)_\phi, \tag{25}$$

where the c^{LV} is defined in Eq. (1). Recall that α^{LV} is the area available in the surface phase per excess mole and is equal to $1/n^{LV}$. For the steady-state circumstances, we shall neglect any changes in α^{LV} with position on the interface. Then Eq. (24) may be written

$$(\kappa^V \nabla T^V - \kappa^L \nabla T^L)_I \cdot \mathbf{i}_r = j_{ev}(h^V - h^L)_I + \frac{n^{LV}\nu_\theta^{LV}c^{LV}}{R_0}\left(\frac{\partial T^{LV}}{\partial \theta}\right)_\phi. \tag{26}$$

The product $n^{LV}c^{LV}$ has been defined as the surface-thermal capacity c_σ. We investigate its value by first assuming that this quantity is constant. After integrating Eq. (26) and making use of Eqs. (19) and (20), one finds

$$c_\sigma = \frac{\dot{Q}_V - \dot{E}_{ev}}{2\pi \int_0^{\theta_m} \nu_\theta^{LV}\left(\frac{\partial T^{LV}}{\partial \theta}\right) R_0 \sin\theta \, d\theta}. \tag{27}$$

The values of the surface-thermal capacity for experiments EV8–EV16 are shown in Fig. 6.

As may be seen there, although Ma changed by a factor of ~5 and the evaporation flux by a factor of ~34, the value of the surface-thermal capacity was not measurably different in any of these nine experiments. The mean surface-thermal capacity for these experiments was 30.6 kJ/(m^2 K) when the interfacial temperature was in the range $-10\ ^\circ\text{C} \leqslant T^{LV} \leqslant 3.5\ ^\circ\text{C}$. The possible error in c_σ is discussed below. In determining the value of c_σ from EV8–EV16, the assumption was made that the viscous dissipation was negligible. Since the same value of c_σ was obtained from each of the these experiments and, as indicated in Table I, the maximum thermocapillary speed increased by a factor ~3, the results seem consistent with this assumption.

When the surface thermal capacity is taken to have the value 30.6 kJ/(m^2 K), the energy required to evaporate the liquid at the measured rate can be compared with that calculated from thermal conduction and thermocapillary convection. After introducing the definition of c_σ into Eq. (26), one finds

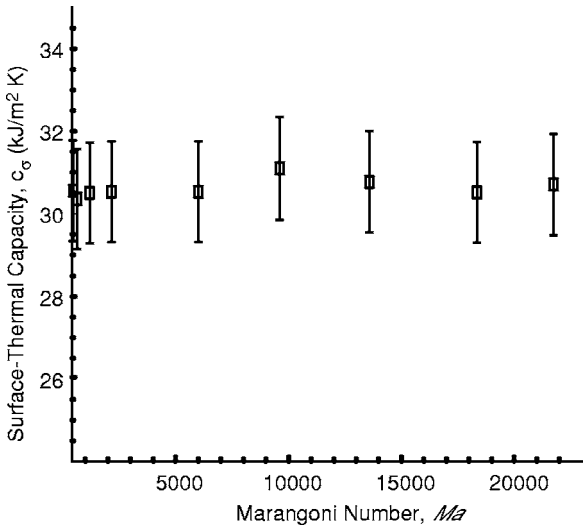

FIG. 6. The "surface thermal capacity" for experiments EV8–EV16 is shown as a function of the Marangoni number. For these experiments, there was thermocapillary convection, but the interface was not turbulent (Tables I and II). Between EV8 and EV16, the evaporation rate increased by a factor of ~34.

$$j_{ev}(h^V - h^L)_I = (\kappa^V \nabla T^V - \kappa^L \nabla T^L)_I \cdot \mathbf{i}_r - \left(\frac{c_\sigma \nu_\theta^{LV}}{R_0}\right)\left(\frac{\partial T^{LV}}{\partial \theta}\right)_\phi. \tag{28}$$

The first term on the right of Eq. (28) represents the thermal energy conducted to the interface from the liquid and vapor phases. As seen in Fig. 4, for experiments EV1–EV6, thermal conduction alone provides the energy required to evaporate the liquid at the measured rate, but as the evaporation rate was progressively increased in EV8–EV16, thermal conduction provided a progressively smaller portion of the energy, reaching only ~60% of the total in EV16.

The second term on the right of Eq. (28) indicates the thermal energy transported along the interface by thermocapillary convection. After making use of Eq. (21), one finds

$$-\left(\frac{c_\sigma \nu_\theta^{LV}}{R_0}\right)\left(\frac{\partial T^{LV}}{\partial \theta}\right)_I = \left(\frac{c_\sigma}{\eta R_0}\right)\left(\frac{d\gamma^{LV}}{dT^{LV}}\right)_I\left(\frac{\partial T^{LV}}{\partial \theta}\right)^2 \ln\left(1 - \frac{\delta_u}{R_0}\right). \tag{29}$$

Since the surface tension of water decreases with increasing temperature and

$$0 < \frac{\delta_u}{R_0} < 1,$$

the second term in Eq. (29) is positive and the energy transport by thermocapillary convection adds to that carried by conduction. The thermal energy carried by the thermocapillary flow comes from heating the funnel throat. The thermal conductivity of stainless steel is more than 20 times that of water, and the throat of the funnel was maintained at ~4 °C,

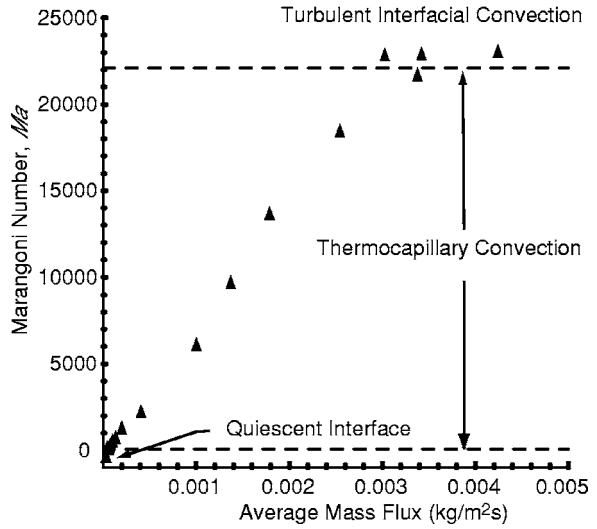

FIG. 7. The Marangoni number plotted against the average evaporation flux indicates two interfacial flow transitions: the first from a quiescent interface to one with thermocapillary convection (see Fig. 5) and the second to turbulent interfacial flow.

the highest temperature in the system. Physically, thermal energy is transported from the funnel throat to the funnel rim through the stainless steel funnel, heating the liquid to give the interfacial temperature profile indicated in Fig. 2. The resulting thermocapillary convection distributes the energy along the interface. As seen in Fig. 4, when the energy transport by both thermocapillary convection—using c_σ equal to 30.6 kJ/(m^2 K)—and by thermal conduction are taken into account conservation of energy is completely satisfied.

The uncertainty in the value of the surface-thermal capacity for each experiment is determined by the possible error in the thermal conduction to the interface, $\Delta(\dot{Q}_N)$; in the total energy transport required to evaporate the liquid at the observed rate, $\Delta(\dot{E}_{ev})$; in the thermocapillary speed $\Delta(\nu_\theta^{LV})$; and in the measured temperature gradient $\Delta(\partial T^{LV}/\partial\theta)$. We take the estimated error in the surface-thermal capacity, $\Delta(c_\sigma)$, for each experiment to be [21,22]

$$\Delta(c_\sigma) = \sqrt{[\Delta(\dot{Q}_N)]^2 + [\Delta(\dot{E}_{ev})]^2 + [\Delta(\nu_\theta^{LV})]^2 + [\Delta(\partial T^{LV}/\partial\theta)]^2}. \tag{30}$$

The value of this estimated error for each of the nine experiments is less than ±2.5%. The error bars in Fig. 6 reflect this relative error. Thus the value of c_σ determined from these experiments is 30.6±0.8 kJ/(m^2 K).

C. Evaporation when Ma > 22,000

For experiments EV17, EV18, and EV19, it was pointed out in [1] that the variables such as the evaporation rate and the vapor-phase pressures bifurcate, although these variables had a one-to-one relation at lower evaporation rates. Also, when Ma is plotted against the average evaporation flux, Fig. 7, the graph indicates a change in flow character for experiments with Ma greater than 22,000, and these experiments correspond to those in which the variables bifurcate. Further, when Ma exceeds 22,000, the power spectrum of the interfacial flow was noted to undergo a change in character [1]. Compared with the experiments having smaller Marangoni numbers, the power spectrum indicated that the frequencies of the flow oscillations formed a continuum and contained new and dominate frequencies. The frequency continuum suggests the presence of eddies in the interfacial flow of new sizes. When the flow is turbulent, it is generally expected the smaller-sized eddies are responsible for the dissipation of energy [23]; thus, the fluid speed in both the $\boldsymbol{i}_\phi$ and $\boldsymbol{i}_\theta$ directions would be important in determining the energy dissipated. Since the measurements indicate that the interfacial temperature profile was axisymmetric [1], we approximate the turbulent interfacial flow as having no significant *mean* flow in the $\boldsymbol{i}_\phi$ direction. We take the expression for ν_θ^{LV} given in Eq. (21) to define the *mean* flow in the $\boldsymbol{i}_\theta$ direction and then determine the mean viscous dissipation. Since α^{LV} has been assumed to be unchanging along the interface, one finds from Eqs. (13) and (25) that

$$(\kappa^V \nabla T^V - \kappa^L \nabla T^L)_I \cdot \boldsymbol{i}_r = j_{ev}(h^V - h^L)_I + \frac{\overline{\nu}_\theta^{LV} c_\sigma}{R_0}\left(\frac{\partial T_I^L}{\partial\theta}\right) + \Phi_I. \tag{31}$$

Since the surface-thermal capacity is indicated not to change significantly over the range of experimental conditions corresponding to $38 < \mathrm{Ma} < 22{,}000$, we assume it has the same value even when the interfacial flow becomes turbulent and over a slightly expanded temperature range $-12\ ^\circ\mathrm{C} \leqslant T^{LV} \leqslant 3.5\ ^\circ\mathrm{C}$. The average value of the local dissipation can be calculated by integrating Eq. (31) over the surface:

$$\overline{\Phi_I} = \frac{\dot{Q}_N - \dot{E}_{ev} - \dot{E}_\sigma}{2\pi R_0^2(1-\cos\theta_m)}, \tag{32}$$

where $\dot{E}_\sigma$, the energy transported by thermocapillary convection, is given by

$$\dot{E}_\sigma = 2\pi c_\sigma \int_0^{\theta_m} \overline{\nu}_\theta^{LV}\left(\frac{\partial T^L}{\partial\theta}\right)_I R_0 \sin\theta\, d\theta. \tag{33}$$

After again making use of Eqs. (22) and (23), Eqs. (15), (16), and (33) may be applied and the results used in Eq. (32) to determine the value of $\bar{\Phi}_I$ for experiments EV17, EV18, and EV19.

In Fig. 8, the calculated values of $\bar{\Phi}_I$ for each of these experiments is plotted against the maximum value of the mean speed, $\overline{\nu}_{\theta M}^{LV}$. As may be seen there, the average energy dissipation increased almost linearly with increasing $\overline{\nu}_{\theta M}^{LV}$. This supports the suggestion in [1] that the interfacial flow induced by the evaporation becomes turbulent at the higher evaporation rates. Also, the effect of the viscous dissipation on evaporation when the interfacial flow becomes turbulent may be seen from Eq. (31) to decrease the evaporation rate. Energy that is transferred into a surface element by thermal conduction and thermocapillary convection goes either into phase change or viscous dissipation. Thus the thermocapillary convection plays a conflicted role: it transports energy that can enhance evaporation, but if Ma exceeds 22,000, not

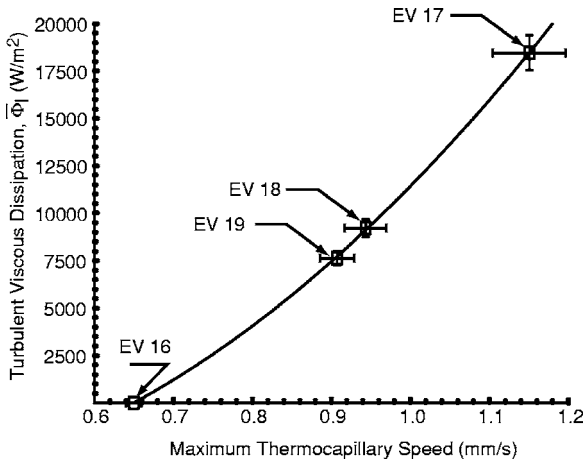

FIG. 8. When the Marangoni number exceeded ~22 000, the interfacial flow was turbulent [1]. This condition was reached in experiments EV17, EV18, and EV19 (Table II). Note that the value of the viscous dissipation correlates with the maximum fluid speed generated by the Marangoni effect.

all of the energy transported goes into evaporation. Some goes into turbulent fluid motion. The fraction of the energy transported by thermocapillary convection, $\dot{E}_\sigma$, that goes into viscous dissipation $\bar{\Phi}_I$ increases as the thermocapillary flow velocity increases. The ratio of $\bar{\Phi}_I/\dot{E}_\sigma$ reaches 0.57 in EV19. Thus only 43% of $\dot{E}_\sigma$ goes into enhancing the evaporation in this turbulent flow circumstance.

V. DISCUSSION AND CONCLUSION

As indicated in Fig. 4, for Ma less than ~100, the interface is apparently quiescent and thermal conduction provides the energy transport required to evaporate the liquid at the measured rate. As Ma and the evaporation rate became progressively larger, in nine independent experiments with Ma reaching 22,000 and the evaporation flux increasing by a factor of ~34, thermal conduction was found to account for a progressively smaller portion of the total energy transported to the interface. Thermal conduction was reduced to approximately 60% before the interfacial flow became turbulent.

In these nine experiments ($100 < \mathrm{Ma} < 22,000$), the thermal conductivity of water became a limiting factor. The temperature of the water at the funnel throat was less than 4 °C, and as a result of evaporative cooling, the temperature was lower still at the liquid-vapor interface. Since water has its maximum density at 4 °C and its density decreases monotonically below 4 °C, the temperature field ensured that there was no buoyancy-driven convection. When both thermocapillary and buoyancy-driven convection are possible, the coupling between them gives rises to convection in the liquid phase [5], but since in our experiments buoyancy-driven convection is not present, the type of convection, sometimes called Marangoni-Bénard, was not present. The fluid velocity in the bulk liquid, $\boldsymbol{\nu}^L$, is simply that produced by the syringe pump.

The convection that did exist below the uniform-temperature layer was completely taken into account by the energy flux vector: $(n^L h^L \boldsymbol{\nu}^L - \kappa^L \boldsymbol{\nabla} T^L)_I$ [see Eq. (12)], but since there was no buoyancy-driven convection and the Reynolds number in the bulk was small ($\mathrm{Re} < 0.01$), the temperature profile in the bulk liquid was very nearly linear (see Fig. 4 of [1]). Thus the energy transport to the bottom of the uniform-temperature layer could be determined by measuring the temperature gradient. The transport across the uniform temperature layer is discussed below.

Since the thermal conductivity of stainless steel is more than 20 times that of water, thermal conduction from the funnel throat to the funnel rim maintained the temperature there at a value greater than that of the water on the center line. This gave rise to the parabolic interfacial temperature profiles, as indicated in Fig. 2. The resulting surface tension gradient produced thermocapillary convection from the funnel rim toward the center line. It was shown in [1] that the mean thermocapillary speed calculated from Eq. (21) was in agreement with that determined by measuring the deflection of a cantilevered flow probe. The fluctuation in the thermocapillary flow is discussed below. The maximum calculated value of the mean thermocapillary speed, $\nu_{\theta M}^{LV}$, for the experiments with Ma in the indicated range is listed in Tables I and II. Note that for Ma equal to 127, the thermocapillary speed was too small to be measured.

When the thermocapillary speed was large enough to be measured, a uniform-temperature layer was observed to be present in the liquid phase immediately below the interface. The average radial speed toward the interface, $\overline{\nu_{I_r}}$ (i.e., $\overline{\boldsymbol{\nu}_I^L \cdot \boldsymbol{i}_r}$), may be determined from the measured total rate of evaporation, J_{ev}, the area of the interface, A_I, and the density n_I^L:

$$\overline{\nu_{I_r}} = \frac{J_{ev}}{A_I n_I^L}.$$

The ratio of the fluid speed parallel and perpendicular to the interface (i.e., $\nu_{\theta M}^{LV}/\overline{\nu_{I_r}}$) for the experiments with $127 < \mathrm{Ma} < 22,000$, ranged from ~200 to ~2,000. Thus the interfacial temperature gradient produced a thermocapillary flow from the funnel rim toward the center line, but because the thermocapillary flow rate is so much larger than the radial flow rate, there was a return flow from the center line toward the funnel rim. Since the liquid on the interface was cooler, and therefore lighter than that below, the penetration of the thermocapillary flow into the bulk would have been resisted by buoyancy and the return flow would have been forced toward the interface. The mixing produced by these two oppositely directed flow streams is suggested to be the cause of the uniform-temperature layer. Also, in the energy and mass balance at the interface, we assumed the energy transported to the bottom of the uniform-temperature layer was transported across this layer to the interface by the mixing in the uniform-temperature layer [see Eqs. (28) and (29)]. In the steady-state circumstance of our experiments, this amounts to assuming that there was no storage of thermal energy in the uniform-temperature layer.

The thermocapillary flow carries thermal energy from the warmer funnel rim and distributes it along the interface. If this convected energy is taken into account, the conservation of energy principle is fully satisfied, provided the surface-thermal capacity c_σ is assigned a value of 30.6 ± 0.8 kJ/(m^2 K) (see Fig. 4) for each of the nine experiments with $127 < \mathrm{Ma} < 22,000$. Thus the surface-thermal capacity acts like a property of the water-vapor interface that does not change significantly even though other properties undergo changes (see below).

The molecular interaction that would give rise to c_σ remains to be established. Its value is larger than would be expected for an equilibrium interface. The volumetric specific heat for bulk water at 0 °C is 4.23×10^3 kJ/(m^3 K). The value this would imply for the surface phase is not clear because (1) the molecular bonding is different in the surface phase than in the bulk, (2) the value of n^{LV} is unknown—recall that $c_\sigma = n^{LV} c^{LV}$ [see Eq. (1)]—and (3) the surface phase that we consider is in disequilibrium with a temperature gradient that causes a surface tension gradient. This gradient gives rise to the observed thermocapillary speed.

The surface-thermal capacity plays a role in the energy transport only if there is thermocapillary convection. Energy transport by this mechanism vanishes if ν_θ^{LV} vanishes [see Eq. (26)]. A recent analysis of the energy transport to the interface of an evaporating liquid, based on classical kinetic theory, has been reported by Bond and Struchtrup [24]. As the authors point out, they neglected surface tension effects; thus, their analysis does not shed light on a molecular interpretation of c_σ.

Analyses of the molecular sources of surface tension have limited themselves to equilibrium circumstances. The molecular interactions that give rise to surface tension, even under equilibrium conditions, are still under discussion. One approach considered is based on the "random network model" of water [25,26]. It has been applied to account for the temperature dependence of surface tension [27]. This model treats water as a continuous network of hydrogen bonds that, on a suitable time scale, can be viewed as a distorted, icelike structure that includes all the molecules in the configuration as members of the network. Energy is viewed as arising from two principal contributions: lattice vibrations of the water molecules about their quasiequilibrium positions and from the deformation of the hydrogen bonds that help determine the quasiequilibrium positions of the molecules. Although a number of assumptions and approximations are required, this approach has been shown to give numerical values of the surface tension over a temperature range between 0 and 30 °C that are within ~10% of the measurements.

The random network model of water can be used to suggest a molecular explanation for the value of c_σ, but first we note the lack of correlations between c_σ and other properties. One of the remarkable characteristics of c_σ is its constancy (see Fig. 6), although during the series of nine experiments, the Marangoni number changed by a factor of 5, the evaporation flux changed by a factor of 34, the temperature discontinuity by a factor of 3.6, and the vapor-phase pressure was reduced from 777 to 301 Pa, and in [13] it is shown that c_σ for water is not sensitive to interface curvature. Thus it would not appear that any of these parameters are controlling in the determination of c_σ. However, as noted in an earlier section, flow fluctuations were observed when a flow probe was used to measure the thermocapillary-generated interfacial speed [1]. In the series of experiments conducted to examine the analytical expression for this speed, Eq. (21), the vapor-phase pressure ranged from 599 to 300 Pa, a range that is similar to that in the nine experiments used to measure c_σ. The fluctuations in the flow speed ranged from ± 0.2 to ± 0.3 mm/s, and the fluctuations in the flow speed were of the same order as the flow speed itself in each experiment. Thus, although the flow fluctuations are large, their magnitude did not change during the course of these experiments, a characteristic that is similar to c_σ. If the random network model of water is valid, one can imagine that the vibrations in a hydrogen-bonded water molecule, about its quasiequilibrium position, would be much larger than under equilibrium conditions, as indicated by the fluctuation to flow probe, when the thermocapillary force pulled the water molecule from one quasiequilibrium position to another. Under near-equilibrium conditions, at a vapor-phase pressure of 820 Pa, no deflection of the flow probe could be measured [1].

When Ma is less than 22,000, the viscous dissipation appears to be negligible, and Eqs. (21) and (28) indicate that thermocapillary convection enhances the rate of evaporation, independently of the sign of $(\partial T_I^L / \partial \theta)$. Evaporation experiments of organic liquids have been recently reported [28] in which the liquid phase was *outside* the surface of curvature and for which $(\partial T_I^L / \partial \theta)$ was *negative*. It was found that the effect of thermocapillary convection was to enhance the evaporation rate. For the experiments we report, the liquid phase was *inside* the surface of curvature and $(\partial T_I^L / \partial \theta)$ was *positive* (see Fig. 2). As indicated in Fig. 4, the effect of the thermocapillary convection was to enhance the rate of water evaporation.

When Ma exceeds 22,000, a transition in the thermocapillary convection occurs (Fig. 7). This transition was also studied with the cantilevered flow probe. The power spectrum of the oscillations indicated a continuum of probe frequencies appeared following this transition, supporting other indications that the interfacial flow became turbulent. Using the inferred value of the surface-thermal capacity, the average value of the viscous dissipation is found to increase almost linearly with the maximum interfacial speed (see Fig. 8). Although thermocapillary convection enhances the evaporation rate for $\mathrm{Ma} < 22,000$, once the flow becomes turbulent, the fraction of the energy associated with thermocapillary convection that goes into phase change is reduced. The remainder goes into viscous dissipation.

ACKNOWLEDGMENTS

This work was supported by the Canadian Space Agency and the Natural Sciences and Engineering Research Council of Canada.

[1] C. A. Ward and Fei Duan, Phys. Rev. E **69**, 056308 (2004).
[2] J. R. A. Pearson, J. Fluid Mech. **4**, 489 (1958).
[3] C. V. Sterling and L. E. Scriven, AIChE J. **5**, 514 (1959).
[4] D. A. Nield, J. Fluid Mech. **19**, 341 (1964).
[5] An-Ti Chai and N. Zhang, Exp. Heat Transfer **11**, 187 (1998).
[6] H. F. Bauer, Ing.-Arch. **52**, 263 (1982).
[7] G. T. Barnes and D. S. Hunter, J. Colloid Interface Sci. **88**, 437 (1982).
[8] H. K. Cammenga, D. Schreiber, G. T. Barnes, and D. S. Hunter, J. Colloid Interface Sci. **98**, 585 (1984).
[9] A. Y. Rednikov, P. Colinet, M. G. Velarde, and J. C. Legros, J. Fluid Mech. **405**, 57 (2000).
[10] J. L. Castillo and M. G. Velarde, J. Fluid Mech. **125**, 463 (1982).
[11] J. Willard Gibbs, Trans. Conn. Acad. Arts Sci. **3**, 108 (1876); in *The Scientific Papers of J. Willard Gibbs*, edited by H. A. Bumstead and R. G. Van Name (Dover, New York, 1961), Vol. 1, p. 219.
[12] C. A. Ward, J. Non-Equilib. Thermodyn. **27**, 289 (2002).
[13] F. Duan, V. K. Badam, F. Durst, and C. A. Ward, following paper, Phys. Rev. E **72**, 056303 (2005).
[14] F. Duan and C. A. Ward, this issue, Phys. Rev. E **72**, 056304 (2005).
[15] C. A. Ward and D. Stanga, Phys. Rev. E **64**, 051509 (2001).
[16] G. Fang and C. A. Ward, Phys. Rev. E **59**, 417 (1999).
[17] C. A. Ward and G. Fang, Phys. Rev. E **59**, 429 (1999).
[18] A. J. H. McGaughey and C. A. Ward, J. Appl. Phys. **91**, 6406 (2002).
[19] S. Popov, A. Melling, F. Durst, and C. A. Ward, Int. J. Heat Mass Transfer **48**, 2299 (2005).
[20] G. Fang and C. A. Ward, Phys. Rev. E **59**, 441 (1999).
[21] A. J. Wheeler and A. R. Ganji, *Introduction to Engineering Experimentation* (Prentice-Hall, Upper Saddle River, NJ, 1996), p. 168.
[22] J. R. Taylor, *An Introduction to Error Analysis: The Study of Uncertainties in Physical Measurements*, 2nd ed. (University Science Books, Sausalito, CA, 1997), p. 187.
[23] L. D. Landau, *Fluid Mechanics* (Pergamon, London, 1959), p. 119.
[24] M. Bond and H. Struchtrup, Phys. Rev. E **70**, 061605 (2004).
[25] S. A. Rice and M. G. Sceats, J. Phys. Chem. **85**, 1108 (1981).
[26] A. R. Henn and W. Kuzmann, J. Phys. Chem. **93**, 3770 (1989).
[27] A. R. Henn, Biophys. Chem. **105**, 533 (2003).
[28] C. Buffone and Khellil Sefiane, Int. J. Multiphase Flow (to be published).